Persistent inward currents in rat ventral horn neurones

Renée D. Theiss[1], Jason J. Kuo[1] and C. J. Heckman[1,2]

Departments of [1]Physiology and [2]Physical Medicine and Rehabilitation, Northwestern University Feinberg School of Medicine, 303 E. Chicago Ave., Chicago, IL 60611, USA

Throughout the mammalian spinal cord, interneurones have been shown to exhibit distinct firing patterns in response to a step of injected current. In this study of ventral horn interneurones in a thick slice preparation of the lumbar cord of 11–19-day-old-rats, four distinct firing patterns were observed and classified as repetitive-firing, repetitive/burst, initial-burst or single-spiking. The hypothesis that a persistent sodium current was the predominant determinant of cell firing behaviour was investigated. A slow voltage ramp was used to assess persistent inward currents (PICs). Cells with repetitive-firing patterns had significantly larger PICs than cells displaying repetitive/burst, initial-burst or single-spiking patterns. Repetitive-firing, repetitive/burst and initial-burst-firing cells were reduced to a single-spiking pattern with the application of riluzole, which also markedly reduced the persistent sodium current. Persistent sodium current was found to account for most of the PIC with only a small contribution from L-type calcium current. These results suggest that the persistent sodium current plays a major role in determining firing patterns in these cells.

(Received 8 November 2006; accepted after revision 6 February 2007; first published online 8 February 2007)
Corresponding author C. J. Heckman: Department of Physiology, M211, 303 E. Chicago Ave., Chicago, IL 60611, USA. Email: c-heckman@northwestern.edu

In the mammalian spinal cord, interneurones have been shown to exhibit distinct firing patterns in response to a pulse of injected current. These patterns range from repetitive to delayed to bursting to single-spiking (Lopez-Garcia & King, 1994; Hochman *et al.* 1997; Garraway & Hochman, 2001; Prescott & De Koninck, 2002; Szucs *et al.* 2003; Theiss & Heckman, 2005). Some of these firing patterns have been hypothesized to uniquely encode different aspects of sensory input (Ruscheweyh & Sandkuhler, 2002; Schneider, 2003; Prescott & De Koninck, 2005). For example, single-spiking cells have been suggested to function as coincidence detectors (Prescott & De Koninck, 2002), while initial-burst cells may encode input strength (Ruscheweyh & Sandkuhler, 2002; Schneider, 2003). In turn, repetitive-firing cells might be more suited for integration, encoding both intensity and duration of the summed input (Prescott & De Koninck, 2002, 2005).

The currents underlying the different firing patterns in spinal interneurones have only begun to be explored. In spinal motoneurones, inward currents that remain on once activated (i.e. do not inactivate or inactivate slowly) appear to play an important role in rhythmic firing (Alaburda *et al.* 2002; Heckman *et al.* 2003; Hultborn *et al.* 2004). These persistent inward currents (PICs) also appear to be important in spinal interneurones. The L-type calcium current seen in motoneurones also produces plateau potentials in deep dorsal horn interneurones (Russo & Hounsgaard, 1996; Morisset & Nagy, 1999, 2000; Voisin & Nagy, 2001; Derjean *et al.* 2005) and ventral horn interneurones (Smith & Perrier, 2006). The persistent sodium current (Na_P) is also important in mammalian motoneurones, contributing to plateau potentials and playing an essential role in initiation of spikes during repetitive firing (Lee & Heckman, 2001; Kuo *et al.* 2006). Consistent with this role, Na_P, in lamina I cells, is substantially larger in repetitive-firing than single-spiking cells (Prescott & De Koninck, 2005). In addition, currents not prevalent in motoneurones are also likely to be important in generating the different interneurone firing patterns. In the dorsal horn, delayed firing has been attributed to an A-like potassium current (Ruscheweyh & Sandkuhler, 2002), and a D-like outward current has been suggested to be responsible for the single-spiking firing pattern (Ruscheweyh & Sandkuhler, 2002).

Based on the difference in firing patterns seen in interneurones and the importance of Na_P for spike initiation (Lee & Heckman, 2001), we hypothesized that differences in Na_P account for the main differences in firing patterns in ventral horn interneurones. Our results, however, do not entirely agree with this hypothesis: blocking Na_P in repetitive-firing cells does produce a single-spiking pattern, but it does not convert them to initial-burst cells. It is probable that contributions of other currents account for the initial-burst pattern.

 DOI: 10.1113/jphysiol.2006.124123

Methods

Slice preparation

All experiments were carried out under full approval from the Northwestern University Animal Care and Use Committee. The lumbar spinal cords of immature Sprague–Dawley rats (P11–P19) were extracted and sliced into 400 μm transverse sections on a vibrating blade microtome (Vibratome 1000Plus, Vibratome Company, St Louis, MO, USA). Two to three days prior to recording, pups were injected I.P. with 0.05 ml of a 2% Fluoro-Gold (Fluorochrome, Denver, CO, USA) solution in 0.9% isotonic saline, to fluorescently label motoneurones. (Pre-ganglionic sympathetic neurones are also labelled by this method of injection.) To extract the spinal cords on the day of recording, the animals were first anaesthetized with 5% isofluorane in O_2 (2 l min^{-1}) for at least 5 min, ensuring deep anaesthesia and suppression of withdrawal reflexes. As previously described (Theiss & Heckman, 2005), the rat pups were decapitated, and the cord was dissected free of the spinal column and embedded in 2.5% w/v agar. The agar block was then affixed to a stainless steel slicing bath with cyanoacrylic adhesive. During dissection and slicing, the cord was completely immersed in a 4–6°C artificial cerebrospinal fluid (aCSF) cutting solution, pH 7.35 when continuously bubbled with 95% : 5% O_2 : CO_2 and containing (mM): sucrose 234.0, KCl 2.5, $CaCl_2$ 0.1, $MgSO_4$ 4.0, HEPES 15.0, glucose 11.0, Na_2HPO_4 1.0. The slices were subsequently incubated for >1 h in a 32–34°C aCSF incubation solution, pH 7.40 when continuously bubbled with 95% : 5% O_2 : CO_2 and containing (mM): NaCl 126.0, KCl 2.5, $CaCl_2$ 2.0, $MgCl_2$ 2.0, $NaHCO_3$ 26.0 and glucose 10.0.

Electrophysiology

Recordings were made with patch electrodes pulled from borosilicate glass (1.5 mm o.d., 1.2 mm i.d., with filament, A-M systems) with resistances of 2–4 MΩ. The internal patch electrode solution, pH 7.3 and osmolarity 270 mOsm, contained (mM): K-gluconate 140.0, $MgCl_2$ 2.0, HEPES 5.0, EGTA 1.1, $CaCl_2$ 0.1, ATP-Mg^{2+} 5.0 and KCl 5.0. Incubated slices were held with a nylon grid to a glass-bottomed bath and continuously perfused with ambient temperature aCSF recording solution, pH 7.40 when bubbled with 95% : 5% O_2 : CO_2 and containing (mM): NaCl 126, NaH_2PO_4 1, KCl 3, $MgSO_4$ 1.5, $CaCl_2$ 2.5, $NaHCO_3$ 26.2, glucose 10, picrotoxin 0.1 (Sigma, St Louis, MO, USA), 2,3-Dioxo-6-nitro-1,2,3,4,-tetra-hydrobenzo[f]quinoxaline-7-sulphonamide disodium salt (NBQX) 0.01 (Tocris, Ellisville, MO, USA), strychnine 0.01 (Sigma) and D-(−)-2-Amino-5-phosphonopentanoic acid (D-AP5) 0.05 (Tocris). Tetrodotoxin (TTX, Tocris) was added to the recording aCSF for a final concentration of 1 μM TTX. Riluzole (Tocris) was dissolved in DMSO and added to the aCSF as a 0.05% DMSO solution. Nifedipine (Sigma) was also dissolved in DMSO and added to the aCSF as a 0.05% DMSO solution with a final concentration of 10 μM nifedipine. Control and drug solutions were bath applied via a gravity-fed Automate perfusion system (San Francisco, CA, USA).

Whole-cell patch recordings were conducted at room temperature using either an Axoclamp 2A or a Multiclamp 700A amplifier (Axon Instruments, Union City, CA, USA). Data were collected at 10 kHz using a 1401 Plus interface (Cambridge Electronic Designs) with CED Signal software and digitally filtered offline. In discontinuous current clamp, firing patterns were determined by injected current steps of various amplitudes. The instantaneous firing frequency–current (F–I) relations were measured from the rhythmic firing evoked by a slow, triangular ramp of linearly rising and falling injected current (as in Theiss & Heckman, 2005). During the current ramp, the ascending and descending phases began at and returned to the same holding current at the same rate. In single-electrode voltage clamp, the current–voltage (I–V) relations (Fig. 1*B*) were constructed from the currents corresponding to a slow, triangular ramp voltage command that typically began and ended at −70 mV and ascended and descended at the same absolute rate, ∼8–16 mV s^{-1} (Fig. 1*A*). Like the current ramp, the ascending and descending phases began at and returned to the baseline holding potential in a linear fashion at the same rate. Previously, slow ramps such as these have been shown to provide a good estimate of steady-state F–I and I–V behaviour in motoneurones (Lee & Heckman, 1998*a*,*b*).

Cell identification

Whole-cell patch recordings were visually guided. Cells were recorded from laminae VII and VIII. Most cells were located in the ventral horn, and a few were located in the deep dorsal horn, though still in lamina VII. For most cells, digital pictures of the soma and limited proximal processes were taken before or during recording using a 40× water immersion objective and 2–4× magnification. In addition, digital pictures of the location of the electrode tip with respect to the outline of the ventral horn were taken post-recording to estimate cell position using a 10× objective at 0.67× magnification. The approximate locations of 67 of these cells are shown in Fig. 2. Motoneurone pools were identified by FluoroGold labelling or by visual inspection of large cell bodies near the ventral border of the grey matter. These motor nuclei were avoided. In avoiding these pools, interneurones located adjacent to or within these areas, such as Renshaw cells, were not adequately sampled.

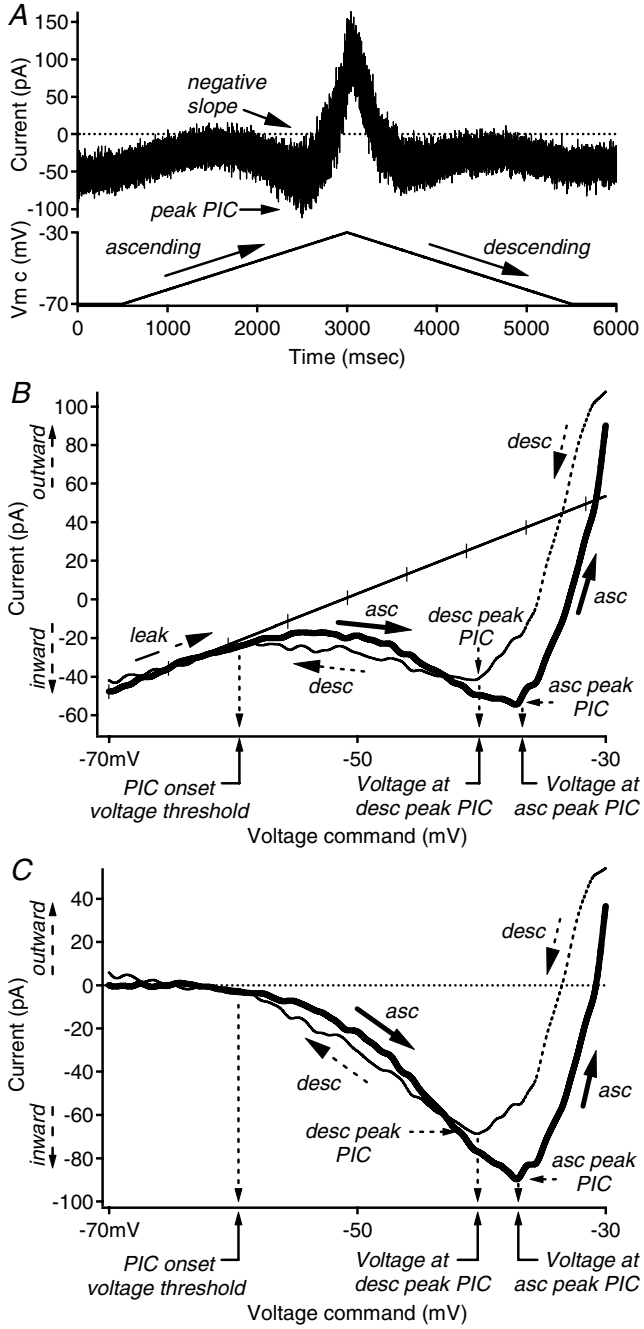

Figure 1. Defining quantification of *I–V* properties
A, raw data example of the current response (top trace, in pA) to a ramp voltage command (bottom trace, in mV) recorded during voltage clamp. Voltage ramps typically began and ended at −70 mV, and ascended and descended at the same absolute rate, ∼8–16 mV s^{-1}. *B*, the current–voltage (*I–V*) relation was constructed by expressing the current trace as a function of the voltage command. The *x* axis is the voltage command (in mV), and the *y* axis is the current response (in pA). The leak conductance is indicated by the hash-marked trace. For convention, outward currents are expressed as positive values, and inward currents are expressed as negative values. *C*, the leak-subtracted *I–V* relation was produced by subtracting the leak conductance from the *I–V* relation in *B*. Peak PIC, voltage at peak PIC and PIC onset are shown and calculated as described in the data analysis section of the Methods. The *x* axis is the voltage command (in mV), and the *y* axis is the current response (in pA). Abbreviations: asc: ascending; desc: descending; leak: leak conductance; PIC: persistent inward current.

As in previous studies of spinal interneurones in *in vitro* preparations (Morisset & Nagy, 1996; Hochman *et al.* 1997; Thurbon *et al.* 1998; Garraway & Hochman, 2001; Szucs *et al.* 2003), it was not possible to distinguish true interneurones, with axons that remained within the cord, from cells whose projections form ascending tracts. Thus, the term 'interneurone', as used here, may include ascending tract projection cells.

Data analysis

Data were analysed offline using IgorPro analysis software (Wavemetrics, Lake Oswego, OR, USA). As previously described (Theiss & Heckman, 2005), cell properties recorded in current clamp were defined as follows:

Resting membrane potential ($V_{m,rest}$) was measured in quiescent cells lacking spontaneous firing while no current was injected. Action potential magnitude or spike height was calculated from the first spike fired to a given input as the difference between peak (overshoot) and baseline membrane potential. Action potential maximum rate of rise was measured at the peak of the first derivative of the local spike voltage trace with respect to time. Action potential (AP) voltage threshold was measured as the point on the first spike generated in response to a ramp of injected current where the rate of rise reached 20% of the maximum. This method provided a good estimation of the inflection point where the spike initiated from the voltage upswing to a depolarizing input or at the end of the afterhyperpolarization (AHP). *F–I* threshold current was defined as the amplitude of the injected current that coincided with the time occurrence of the voltage threshold for the first spike on the ascending phase of the current ramp. *F–I* gain was calculated from the slope of the regression line from the 4th interspike interval through the most linear portion of the ascending leg of the relationship. *F–I* current hysteresis was calculated as the difference between the *F–I* threshold current of the last spike and the *F–I* threshold current of the first spike. In this manner, when the offset of firing occurred at a higher amplitude of current than the onset, the hysteresis value was considered to be positive. When the offset of firing was at a lower current than the onset, the current hysteresis value was negative. Spontaneous firing frequency was measured as the steady-state frequency when injected current (I_{inj}) equalled 0 pA. When spontaneous firing was present, membrane potential was held subthreshold with injected hyperpolarizing current for measurements of other properties. The AHP amplitude was calculated

from the first spike fired to a ramp input as the difference between the local voltage threshold and the local minimum. When no spikes were fired to a ramp input, the AHP was calculated in the same manner from a low-amplitude injected current step that produced a single action potential.

Cell properties recorded in voltage clamp were defined as follows. The leak conductance (G_{leak}) was extrapolated from the slope of a regression line fit to the sub-threshold region of the *I–V* relation (Fig. 1*B*). Leak conductance measured in voltage clamp is analogous to input conductance that is measured in current clamp. The leak conductance was then subtracted from the raw *I–V* relations to produce the leak-subtracted *I–V* relation from which the following measurements were then made (Fig. 1*C*). Peak persistent inward current amplitude (PIC amplitude) was measured from the minimum deflection in the ascending and descending phases of the leak-subtracted *I–V* relation. These measurements were correspondingly named ascending PIC amplitude and descending PIC amplitude. In our convention, net inward currents were expressed as negative current values, and outward currents were expressed as positive current values. Net inward PIC values therefore are reported as negative numbers. The voltage at peak PIC was determined by the point on the voltage command that coincided with the time occurrence of the PIC peak amplitude. Again, these measurements were taken on both the ascending and descending phases of the *I–V* relation and subsequently labelled as ascending or descending. PIC onset voltage was calculated from the ascending phase as the voltage where the leak-subtracted current traces reached 1% of the peak PIC amplitude. Note: the amplitudes of PICs in single-spiking cells were so small that measurements of the voltage at peak PIC and PIC onset voltage were difficult to determine. Negative slope regions in the ascending *I–V* relation were noted (Fig. 1*A*). A negative slope region is apparent when the PIC is able to overcome the leak conductance. PIC hysteresis was calculated as the difference between ascending and descending phases' voltages at peak PIC (PIC voltage hysteresis) or the difference between the ascending and descending phases' peak PIC amplitude (PIC current hysteresis). In our convention, a positive voltage hysteresis value indicates that the ascending peak PIC voltage was depolarized to the descending peak PIC voltage, while a negative voltage hysteresis value indicates that the descending peak was depolarized to the ascending value. Likewise, a positive current hysteresis value indicates that the ascending peak PIC amplitude was greater than the descending peak PIC amplitude, and a negative current hysteresis value indicates that the ascending peak PIC amplitude was less than the descending peak PIC amplitude.

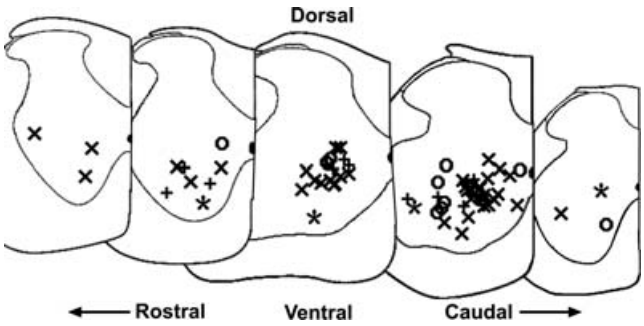

Figure 2. Location of recorded cells
The locations of 67 of the recorded cells were estimated from postrecording digital pictures of electrode tip position (see Methods, cell identification). Rostral to caudal locations are shown left to right; dorsal is to the top and ventral is to the bottom. The medial side of the slice half is indicated with a vertical line on the right side of each slice, with the central canal shown as a darkened half oval. Firing patterns of cells are marked as follows: Repetitive-firing: ×; repetitive-burst: ○; initial-burst: +'; single-spiking: *.

The contribution of persistent sodium (Na_P) conductances to the ascending PIC amplitude was determined by the application of riluzole and TTX. Because of the slow rate of rise of the voltage command, transient sodium currents were inactivated (Crill, 1996), leaving only the persistent sodium component that is sensitive to TTX. It is of note that unlike many studies of persistent sodium where extracellular sodium concentration is decreased to improve clamp control, we used normal values of sodium concentration to allow direct comparisons between *I–V* and *F–I* parameters. The contribution of L-type calcium conductances to the PIC was assessed as well with the application of 10 μM nifedipine. For each cell, the contribution of these persistent currents was calculated as the difference between the control and drug current values at the average control voltage at peak PIC. For convention, these differences in currents are reported as positive values. The effects of riluzole were then expressed as a percentage of the TTX-sensitive PIC. To evaluate the contribution of L-type calcium currents, the effects of nifedipine were calculated as the difference between the TTX-sensitive current and the TTX + nifedipine-sensitive currents and then expressed as a percentage of the total TTX + nifedipine current.

Statistical analyses were performed using IgorPro, Excel (Microsoft Corporation, Redmond, WA, USA) and SPSS (SPSS Inc., Chicago, IL, USA). The α level of significance for unpaired, two-tailed Student's *t*-tests and significant difference from 0 for regression line slopes was set at $P = 0.05$, unless otherwise noted. A conservative Bonferroni correction was used for multiple comparisons, i.e. P/t_n, where t_n = number of tests. For significant difference between measurement for the four groups of cells displaying the four different firing patterns, $t_n = 3$

Table 1. Interneurone properties: summary of intrinsic properties recorded from 86 interneurones in the ventral horn of the lumbar spinal cord

Property	All	Fully repetitive	Repetitive/burst	Initial-burst	Single-spiking	Significance
Age (days)	15.0 ± 1.5 $n = 76$	14.8 ± 1.6 $n = 45$	15.4 ± 1.0 $n = 13$	15.6 ± 1.5 $n = 14$	14.3 ± 2.2 $n = 4$	—
$V_{m,rest}$ (mV)	-55 ± 8 $n = 26$	-54 ± 7 $n = 11$	-52 ± 4 $n = 5$	-54 ± 9 $n = 8$	—	—
Overshoot (mV)	25.6 ± 8.1 $n = 86$	26.0 ± 8.2 $n = 52$	25.3 ± 8.7 $n = 15$	24.3 ± 7.4 $n = 15$	26.5 ± 10.0 $n = 4$	—
Rate of Rise (mV s^{-1})	166.5 ± 47.7 $n = 86$	172.7 ± 48.3 $n = 52$	140.6 ± 41.1 $n = 15$	167.6 ± 43.6 $n = 15$	179.4 ± 61.7 $n = 4$	r::r/b*
AP V_{thresh} (mV)	-36.8 ± 5.1 $n = 77$	-38.2 ± 4.9 $n = 52$	-34.2 ± 4.6 $n = 15$	-33.9 ± 4.1 $n = 9$	—	r::r/b** r::b*
F–I thresh curr (pA)	10 ± 201 $n = 74$	-18 ± 67 $n = 51$	-9 ± 46 $n = 15$	25 ± 42 $n = 7$	—	—
F–I gain (Hz nA^{-1})	214 ± 120 $n = 64$	210 ± 119 $n = 51$	214 ± 112 $n = 12$	—	—	—
F–I curr hyst (pA)	41 ± 36 $n = 64$	40 ± 30 $n = 51$	51 ± 59 $n = 10$	18 ± 29 $n = 3$	—	—
AHP amplitude (mV)	21.0 ± 3.9 $n = 78$	20.3 ± 3.3 $n = 52$	21.0 ± 4.1 $n = 15$	22.3 ± 5.1 $n = 10$	—	—
G_{leak} (nS)	4.2 ± 4.1 $n = 70$	3.8 ± 3.1 $n = 42$	2.9 ± 2.2 $n = 13$	4.0 ± 1.6 $n = 12$	15.6 ± 11.1 $n = 3$	—
PIC ampl asc (pA)	-52 ± 62 $n = 69$	-73 ± 72 $n = 41$	-22 ± 14 $n = 13$	-22 ± 28 $n = 12$	-12 ± 18 $n = 3$	r::r/b‡‡, r::b††, r::s†
V at peak PIC asc (mV)	-42.0 ± 6.9 $n = 67$	-39.7 ± 4 $n = 41$	-40.0 ± 3.6 $n = 12$	-48.9 ± 5.5 $n = 12$	—	r::b‡‡, r/b::b‡
PIC ampl desc (pA)	-16 ± 39 $n = 69$	-19 ± 49 $n = 42$	-12 ± 14 $n = 12$	-9 ± 21 $n = 12$	-18 ± 17 $n = 3$	—
V at peak PIC desc (mV)	-47.1 ± 8.6 $n = 67$	-44.6 ± 9.0 $n = 42$	-49.1 ± 7.3 $n = 11$	-53.0 ± 4.6 $n = 12$	—	r::b‡‡
PIC onset voltage (mV)	-58.3 ± 4.9 $n = 68$	-58.0 ± 5.0 $n = 42$	-56.2 ± 5.6 $n = 12$	-60.4 ± 2.4 $n = 12$	—	—
PIC V_{hyst} (mV)	5.0 ± 7.9 $n = 66$	4.8 ± 7.6 $n = 41$	9.1 ± 7.4 $n = 11$	4.1 ± 5.7 $n = 12$	—	—
PIC I_{hyst} (pA)	36 ± 70 $n = 68$	53 ± 86 $n = 41$	10 ± 10 $n = 12$	12 ± 14 $n = 12$	-6 ± 22 $n = 3$	r::r/b†, r::b†, r::s*

See Methods for definitions of each parameter. Values are listed as mean ± S.D. Parameters (properties) with less than three measurements are not included in the table. Significance: significant differences between firing types; r::r/b: repetitive-firing compared to repetitive/burst, r::b: repetitive-firing compared to initial-burst; r::s: repetitive-firing compared to single-spiking; r/b::b: repetitive/burst compared to initial-burst, r/b::s: repetitive/burst compared to single-spiking, b::s: initial-burst compared to single-spiking; *n*: number of observations; $V_{m,rest}$: resting membrane potential in quiescent cells only; AP V_{thresh}: action potential voltage threshold; *F–I*: frequency–current relation; *F–I* thresh curr: *F–I* threshold current; *F–I* curr hyst: *F–I* current hysteresis; G_{leak}: leak conductance; asc: ascending; desc: descending; PIC: persistent inward current; PIC ampl: peak PIC amplitude; *V* at peak PIC: voltage at peak PIC; PIC V_{hyst}: PIC voltage hysteresis; PIC I_{hyst}: PIC current hysteresis. $^*P < 0.0167$, $^{**}P < 0.01$, †$P < 0.005$, ††$P < 0.001$, ‡$P < 0.0005$, ‡‡$P < 0.0001$.

and the level of significance was adjusted to $P = 0.05/3$, or 0.017.

Results

Electrophysiological data characterizing the persistent currents underlying different firing patterns of ventral horn interneurones were collected using the whole-cell patch configuration in 400 μm transverse slices from the lumbar spinal cords of immature Sprague–Dawley rats (P11–P19). All fast synaptic transmission was blocked. A sample of 86 cells was recorded from laminae VII and VIII, while carefully avoiding the motor nuclei (see Methods). On average, stable recordings were maintained for 35 min. An overview summary of the current- and voltage-clamp measurements is presented in Table 1.

Cells defined by their firing patterns

As in previous studies (Szucs *et al.* 2003; Theiss & Heckman, 2005), ventral horn spinal interneurones displayed distinct firing responses to injected current pulses of varying amplitudes. Most cells displayed repetitive firing (77.9%, $n = 67$, Fig. 3*A*), but significant numbers also responded with an initial-burst firing pattern, i.e. where firing was not maintained through the entire 1 s input (17.4%, $n = 15$, Fig. 3*B*) and a small number exhibited a single-spiking firing pattern (4.6%, $n = 4$, Fig. 3*C*). The convention of naming for these firing patterns was largely based on naming and description from previous studies (e.g. Prescott & De Koninck, 2002; Lopez-Garcia & King, 1994; Hochman *et al.* 1997; Garraway & Hochman, 2001; Szucs *et al.* 2003; Theiss & Heckman, 2005).

In addition, some of the repetitive-firing pattern cells (15/67) were capable of both initial-burst (Fig. 3*Da*) and repetitive-firing patterns (Fig. 3*Db*), depending on input level, and were classified as 'repetitive/burst' cells. In contrast, fully repetitive-firing cells exhibited repetitive firing to a broad range of input levels, and initial-burst cells did not exhibit repetitive patterns at any input level.

Within the repetitive/burst-patterned group, the switch between repetitive or burst behaviours varied from cell to cell. In six repetitive/burst cells, bursts occurred at low input levels and repetitive firing at high levels. In four cells, the opposite occurred, with bursts at higher levels and repetitive firing at lower levels. The other five (of the total of 15) repetitive/burst cells exhibited a narrow region for repetitive firing, with bursting below and above that level. Further work is required to analyse the mechanisms of these differences, but as a group, repetitive/burst cells exhibited clear differences from repetitive-firing and from initial-burst cells during voltage clamp (see below), and thus were separated as a distinct firing type. Overall, this sample of ventral interneurones exhibited four basic types of firing patterns, fully repetitive ($n = 52$, 60.5%), repetitive/burst ($n = 15$, 17.4%), initial-burst ($n = 15$, 17.4%) and single-spiking ($n = 4$, 4.7%).

As in our previous study (Theiss & Heckman, 2005), significant differences existed between the firing types with respect to several other firing properties. On average, fully repetitive-firing cells had significantly higher spike rates of rise than repetitive/burst cells ($P = 0.0167$). Fully repetitive-firing cells also had more hyperpolarized AP voltage thresholds than both repetitive/burst

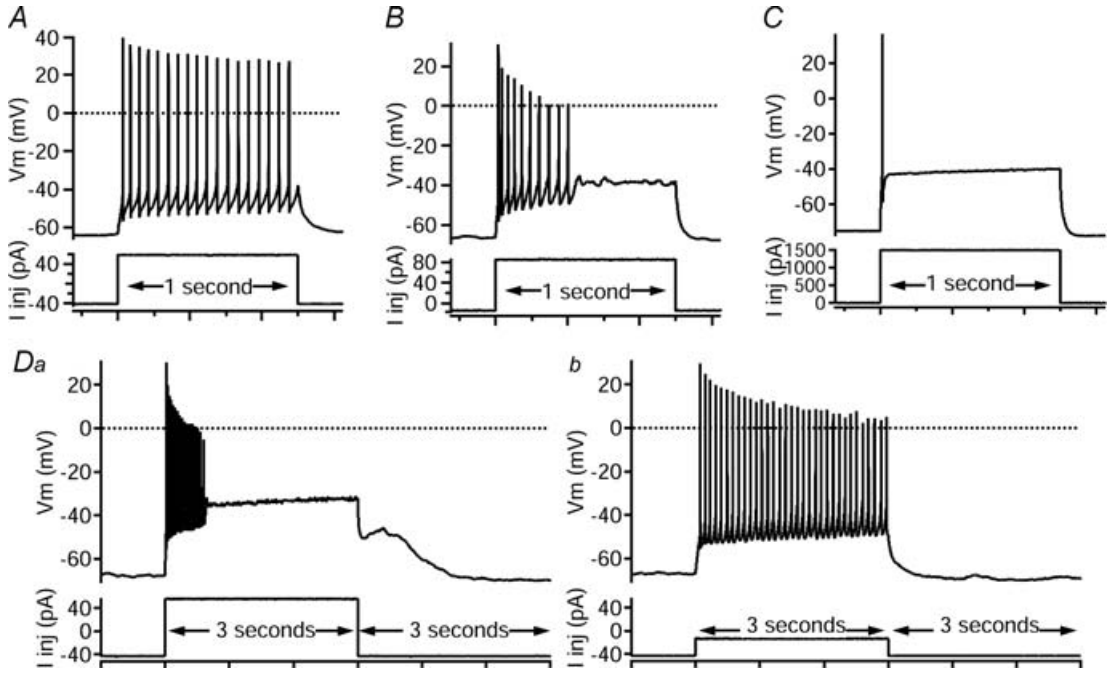

Figure 3. Different firing patterns to depolarizing current pulses
Square current pulses (bottom traces, injected current, I_{inj} in pA), 1 s (*A*–*C*) or 3 s (*D*) in duration, elicited distinct firing responses in different cells (top traces, membrane potential, V_m in mV). *A*, repetitive-firing: the majority of cells recorded (60.5%) fired repetitively through the entire pulse of injected current. *B*, initial-burst: a quickly adapting, non-resurgent burst of spikes that did not persist through the entire 1 s pulse characterized 17.4% of the cells. *C*, single-spiking: even with large-amplitude current steps, 4.7% of the cells fired only 1–2 spikes during the 1 s input. *D*, repetitive/burst: an example of one of the repetitive/burst cells (17.4%) that was capable of both initial-burst (*Da*) and repetitive-firing (*Db*) in response to depolarizing, square-injected current pulses of different amplitudes (bottom traces, in pA).

and initial-burst cells ($P < 0.01$ and $P = 0.0167$, respectively). Additionally, fully repetitive-firing cells had a greater tendency for spontaneous firing (39/51 cells) than repetitive/burst (9/14), initial-burst (3/12) and single-spiking cells (0/4). All of these differences suggest that repetitive-firing cells are more easily excited by sustained inputs than the other types of ventral horn interneurones.

Differences in current–voltage relations

Voltage-clamp studies were performed to assess the differences in currents among the distinct types of firing behaviour in current clamp. The net currents in each cell were assessed from the current–voltage (*I–V*) relation evoked by slow (8–16 mV s^{-1}), linearly increasing and decreasing voltage commands (Fig. 1*A*). Because of the slow rate of rise of the voltage command, transient inward currents underlying the action potential activate and then rapidly inactivate, so that only persistent currents remain. This is the standard method for measuring Na_P and other PICs as well for constructing quasi-steady-state *I–V* functions (Crill, 1996). A negative slope region in the ascending *I–V* function reflects the presence of a PIC large enough to overcome the leak conductance. Voltage-clamp data were obtained in 42 repetitive-firing cells, of which 26 exhibited a negative slope (Fig. 4*A*) and 16 did not (Fig. 4*B*). Additionally, 5/13 repetitive/burst cells and 1/12 initial-burst cells displayed a negative slope region, but no single-spiking cells had negative slopes (0/3). These differences in the presence of negative slope suggest the existence of differences in PIC amplitude among the different cell types.

Within the fully repetitive-firing group, cells with a negative slope region had, on average, significantly higher spike heights ($P < 0.005$), higher spike rates of rise ($P < 0.01$), smaller *F–I* current hysteresis values ($P < 0.005$) and a greater tendency for spontaneous firing (24/26, compared to 8/15 repetitive cells without a negative slope region). Most of these differences are consistent with a larger Na^+ current in cells with negative *I–V* slopes, suggesting that Na_P plays a major role in determining PIC amplitude.

Differences in PIC amplitudes

Measurements of the peak amplitude of the PIC on the ascending phase of the *I–V* relation revealed striking differences between the firing types (Fig. 5 and see Table 1). Repetitive-firing cells had the largest PIC amplitudes (Fig. 5*A*), while repetitive/burst and initial-burst cells had moderate PIC amplitudes (Fig. 5*B* and *C*, respectively). The single-spiking cells exhibited little or no PIC (Fig. 5*D*) but the sample size was small. The PIC amplitude of fully repetitive-firing cells was significantly greater (−73 pA, Table 1) than repetitive/burst cells (−22 pA, $P < 0.0001$), initial-burst cells (−22 pA; $P < 0.001$) and single-spiking cells (−12 pA; $P < 0.005$). There were no significant differences in ascending PIC amplitude, however, between the repetitive/burst, initial-burst and single-spiking cells. Thus, the PIC amplitude exhibited an overall pattern of being large in cells with strong repetitive firing compared to all three other cell types.

The amplitude of the PIC was smaller on the descending phase of the *I–V* relation, compared to the ascending phase (a positive current hysteresis; Table 1), in the majority, 91%, of cells (62/68). This behaviour is consistent with that seen in spinal motoneurones (Lee & Heckman, 1998*a*; Li *et al.* 2004) and probably reflects significant slow inactivation in the PIC. The descending peak for the PIC did not covary with firing type as clearly as did the ascending PIC. There were, however, significant differences in the relative amplitude of the descending PIC compared to the ascending PIC. These differences tracked the differences in ascending PIC amplitude noted above: repetitive-firing cells had significantly larger ascending/descending differences than repetitive/burst, initial-burst and single-spiking cells ($P < 0.005$, $P < 0.005$ and $P = 0.013$, respectively). In spinal motoneurones, the component of the PIC due to L-type calcium currents exhibits less slow inactivation than does the component due to Na_P (Lee & Heckman, 1999; Li & Bennett, 2003; Li *et al.* 2004). Thus, the large reduction in PIC amplitude on the descending phase suggests that the ascending PIC in ventral horn interneurones is dominated by Na_P.

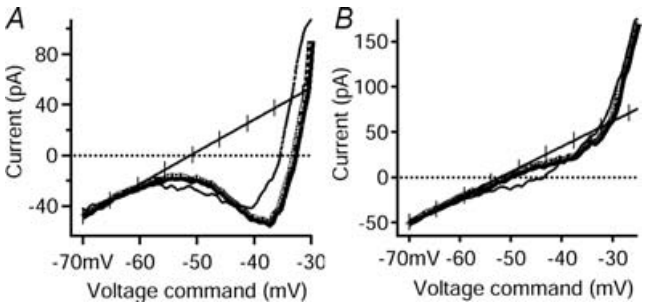

Figure 4. Variations in *I–V* relation features among repetitive-firing cells
Among the repetitive-firing cells, the non-leak-subtracted (or raw) *I–V* relations showed differences in the ascending slope as the peak PIC was approached. In both panels, ascending traces are thick lines, and descending traces are thin lines. The line of leak conductance is hash-marked. The voltage command is shown on the *x* axis, and the resulting current is shown on the *y* axis. *A*, in 26 of 42 fully repetitive-firing cells, a negative slope region was seen as the peak PIC was approached, as shown in this example. *B*, in 16 of 42 fully repetitive-firing cells, no negative slope region was seen, as shown in this example.

Differences in PIC activation voltages

The amplitude of the PIC is a key parameter affecting cell-firing behaviour, but its voltage range for activation is also important (cf. Heckman *et al.* 2003, 2005). In repetitive-firing, repetitive/burst and initial-burst cells, the voltage for onset of the PIC (∼ −56 to −60 mV; see Table 1) was substantially hyperpolarized compared to the voltage threshold for the action potential (∼ −38 to −34 mV; Table 1). The voltage for the peak amplitude of the PIC (∼ −40 to −49 mV; Table 1) was of course more depolarized than that of its onset, but nonetheless still hyperpolarized compared to spike threshold. Thus, the PIC is likely to be strongly activated whenever these cells are producing repetitive firing or bursts.

When considering these results in more detail, significant differences emerge between firing types. As noted previously (Fig. 5), repetitive/burst cells had PIC amplitudes that were similar to those of initial-burst cells, but smaller than those of repetitive-firing cells. This suggests the repetitive/burst cells could be lumped together

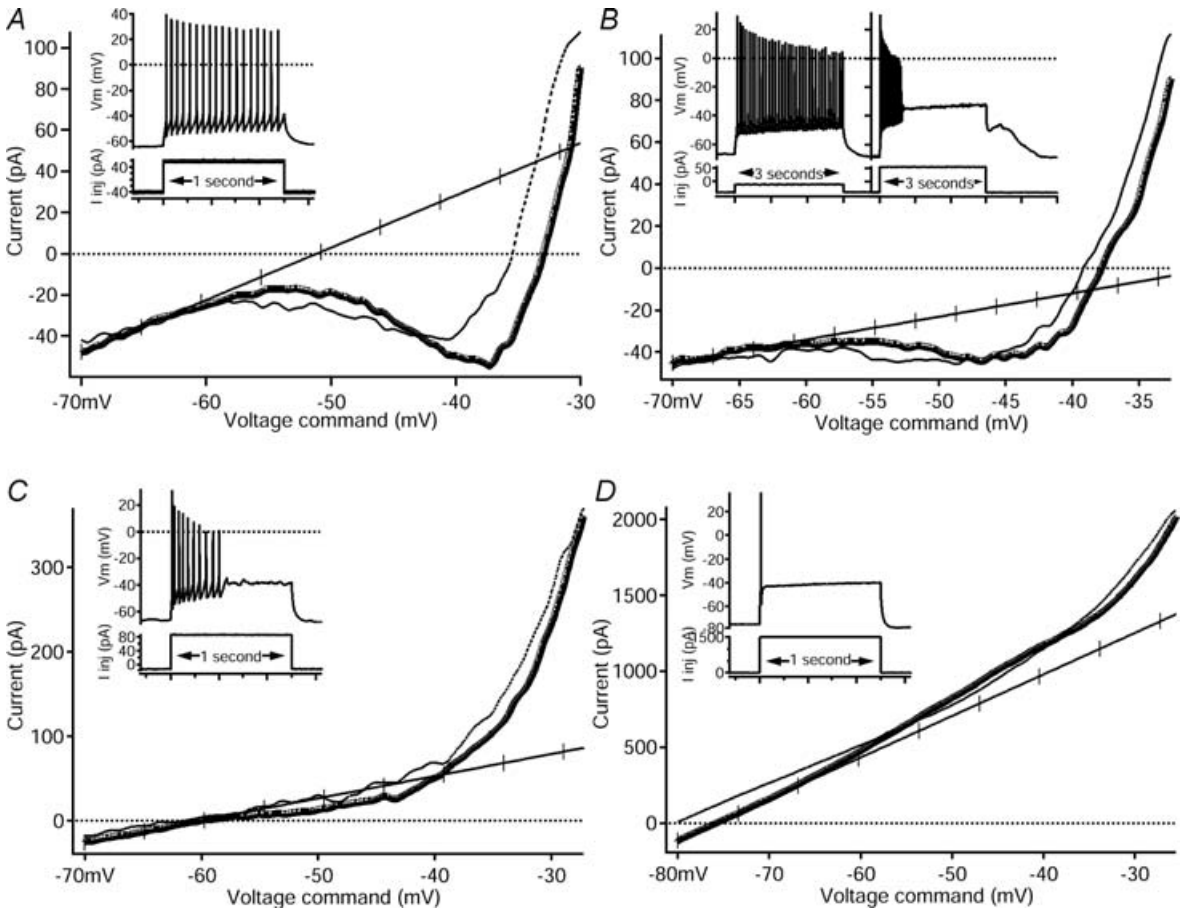

Figure 5. Comparison of *I–V* relations among repetitive-firing, repetitive/burst, initial-burst and single-spiking cells
In all panels, insets are from Fig. 3 and show the firing pattern (top trace, membrane potential, V_m, in mV) in response to a depolarizing, square pulse of injected current (bottom trace, injected current, I_{inj}, in pA) that corresponds to the *I–V* relation. On all *I–V* traces, the voltage command is on the *x* axis and the current is on the *y* axis. (Note: the *y* axes scales are different in each example.) Ascending phases of the *I–V* are shown with thick lines, and descending phases are shown with thin lines. The line of leak conductance is hash-marked. *A*, this fully repetitive-firing cell responded with sustained firing (see inset, also Fig. 3*A*) to a depolarizing input. The *I–V* relation (same cell from Figs 1 and 4*A*) revealed a large PIC with a negative slope region. *B*, this repetitive/burst cell displayed the characteristic repetitive firing to one depolarizing input and burst firing to another (see inset, also Fig. 3*D*). A moderate-amplitude PIC with a negative slope was seen in the *I–V* relation of this cell. *C*, this initial-burst cell responded with a brief burst of spikes (see inset, also Fig. 3*B*) to a depolarizing input. A moderate-amplitude PIC with no negative slope was seen in the *I–V* relation. Note that the current and voltage scales are larger than in *A* and *B*. *D*, the single-spiking cell (see inset, also Fig. 3*C*) fired only one spike to a depolarizing input. No net inward currents were seen in the *I–V* relation, resulting in a 0 pA PIC. Note that the current and voltage scales are larger than in *A*, *B* and *C*.

with initial-burst cells. When the voltages for the onset and for the peak of the PIC were assessed, however, repetitive/burst cells were found to match repetitive-firing cells more closely than initial-burst cells. The voltage at peak PIC amplitude for repetitive (-39.7 ± 4.0 mV; Table 1) and repetitive/burst cells (-40.0 ± 3.6 mV; Table 1) were not significantly different from each other but were both significantly more depolarized than the voltage for initial-burst cells (-48.9 ± 5.5 mV; Table 1). Overall, repetitive/burst cells have PIC characteristics that are shared with both repetitive-firing and initial-burst cells, matching the repetitive-firing cells in PIC voltage range but more closely linked to the initial-burst cells for PIC amplitude.

Contribution of persistent sodium currents

In the introduction, we formulate the hypothesis that Na_P current plays a major role in determining the differences in firing patterns among the classes of firing patterns in the interneurones of this study. From this hypothesis, we would predict that (1) most of the PIC should be due to Na_P instead of an L-type calcium current; and (2) progressive pharmacological block of the Na_P current should be able to convert interneurones with repetitive-firing patterns first into initial-burst and then to single-spiking patterns. To assess the contribution of Na_P conductances to the PICs in interneurones, riluzole, which blocks the persistent component of the total sodium current more strongly than the transient component (Urbani & Belluzzi, 2000; Ptak *et al.* 2005), was bath applied to 18 cells. TTX, which blocks all TTX-sensitive sodium currents, was also applied after riluzole ($n = 16$), or without previous riluzole ($n = 1$) to quantify the total amplitude of Na_P. These Na_P blockers were applied to fully repetitive-firing cells ($n = 9$), repetitive/burst cells (total: $n = 4$; riluzole: $n = 4/4$, riluzole and TTX: $n = 3/4$) and initial-burst-firing cells (total: $n = 6$; riluzole and TTX: $n = 5$, TTX without riluzole: $n = 1$). A concentration of 1 μM riluzole was insufficient to block repetitive firing ($n = 2$), but 5 μM (total: $n = 15$; subsequent to 1 μM: $n = 2$) and 10 μM ($n = 3$) reduced rhythmic or burst firing to 1–3 spikes. After repetitive firing was inhibited by riluzole administration, 1 μM TTX was applied until the remaining spike was eliminated. Several current steps of increasing amplitude were applied to ensure that the threshold for spike generation had not just increased, but that all spikes were indeed blocked by TTX. Total Na_P was calculated as the average difference between the amplitude of the control PIC and the current measured on the drug *I–V* that corresponded to the voltage at the control peak PIC (see Methods).

On average, 5 μM riluzole blocked 69.5% of the TTX-sensitive Na_P current (ascending; total: $n = 14$; fully repetitive-firing: $n = 6$, repetitive/burst: $n = 3$, initial-burst: $n = 4$) and 10 μM riluzole blocked 74.3% of the ascending, TTX-sensitive Na_P current ($n = 2$, both fully repetitive-firing cells). Riluzole, at 5 μM, blocked a larger percentage of Na_P on the descending phase of the *I–V* relation (97.2%, $n = 14$), while the 10 μM concentration blocked a percentage similar to the ascending phase (70.7%, $n = 2$). These percentages were not significantly different when divided into firing types.

Examples of changes in rhythmic firing and corresponding changes in PIC amplitude are shown in Figs 6, 7 and 8. Reducing Na_P with 5 μM riluzole converted the repetitive-firing (Fig. 6), repetitive/burst (Fig. 7) and initial-burst (Fig. 8) cells to a single-spiking pattern and decreased the corresponding PIC amplitudes on both the ascending and descending phases of the *I–V* relations. This reduction of firing to a single spike was not the result of inactivation of transient sodium currents. As illustrated in Fig. 9, riluzole-affected cells still fired to short steps superimposed on a ramp input. The lack of firing to the ramp without steps seen in Fig. 9 illustrates another important point. Although Na_P provides a substantial subthreshold depolarization (e.g. Taddese & Bean, 2002), loss of this depolarization was not the primary mechanism of loss of repetitive firing. Removing Na_P is not equivalent to removing a steady current; it is not simply an offset. As shown in Fig. 9, the current amplitude attained during the later portion of the ramp far exceeded the amount of current required to initiate repetitive firing in the control condition before riluzole application. In addition, when steps were superimposed on the ramp, the amplitude of current at which the first spike was produced (see dashed line on Fig. 9) was exceeded at the later portion of the ramp without steps, though no spikes were produced at that current. These results for ramps and superimposed steps were consistent across all cells tested ($n = 10$). These results strongly support an essential role for Na_P in spike initiation during repetitive firing in ventral interneurones, just as seen in motoneurones (Lee & Heckman, 2001; Kuo *et al.* 2006).

An interesting result was that blocking Na_P did not convert repetitive-firing cells to initial-burst cells. Instead, as riluzole application progressed, repetitive-firing cells displayed a downward shift in the frequency-time (*f–t*) relation during a step, maintaining the same profile, but decreasing the initial and steady-state portions of the adapting firing frequency (Fig. 10*A*, $n = 8$ of 9 tested). This downward shift was in contrast to changes in the initial-burst cells, where the *f–t* relations showed that the initial high frequency was maintained, but the slope of the adaptation increased (Fig. 10*B*, $n = 4$ of 4 tested). This result is consistent with previous studies indicating that initial-burst behaviour may be due to T-type Ca^{2+} or other currents (Ryu & Randic, 1990; Russo & Hounsgaard,

1996; Schneider, 2003) (see Discussion). Thus, while Na_P did account for most of the total PIC in the different cell types, and while suppression of Na_P did convert both repetitive-firing and initial-burst cells to single-spiking cells, differences in Na_P alone are not sufficient to account for the difference between repetitive-firing and initial-burst cells. The results showing maintenance of the spike frequency adaptation profile in our repetitive-firing interneurones was similar to the results seen in juvenile mouse motoneurones after riluzole application (Miles *et al.* 2005). The *f–t* relations of repetitive/burst cells were tracked only in three cells. In all three, when the input was adjusted to produce repetitive firing, results were similar to those for repetitive-firing cells, i.e. the repetitive profile was maintained until failure (Fig. 10*C*).

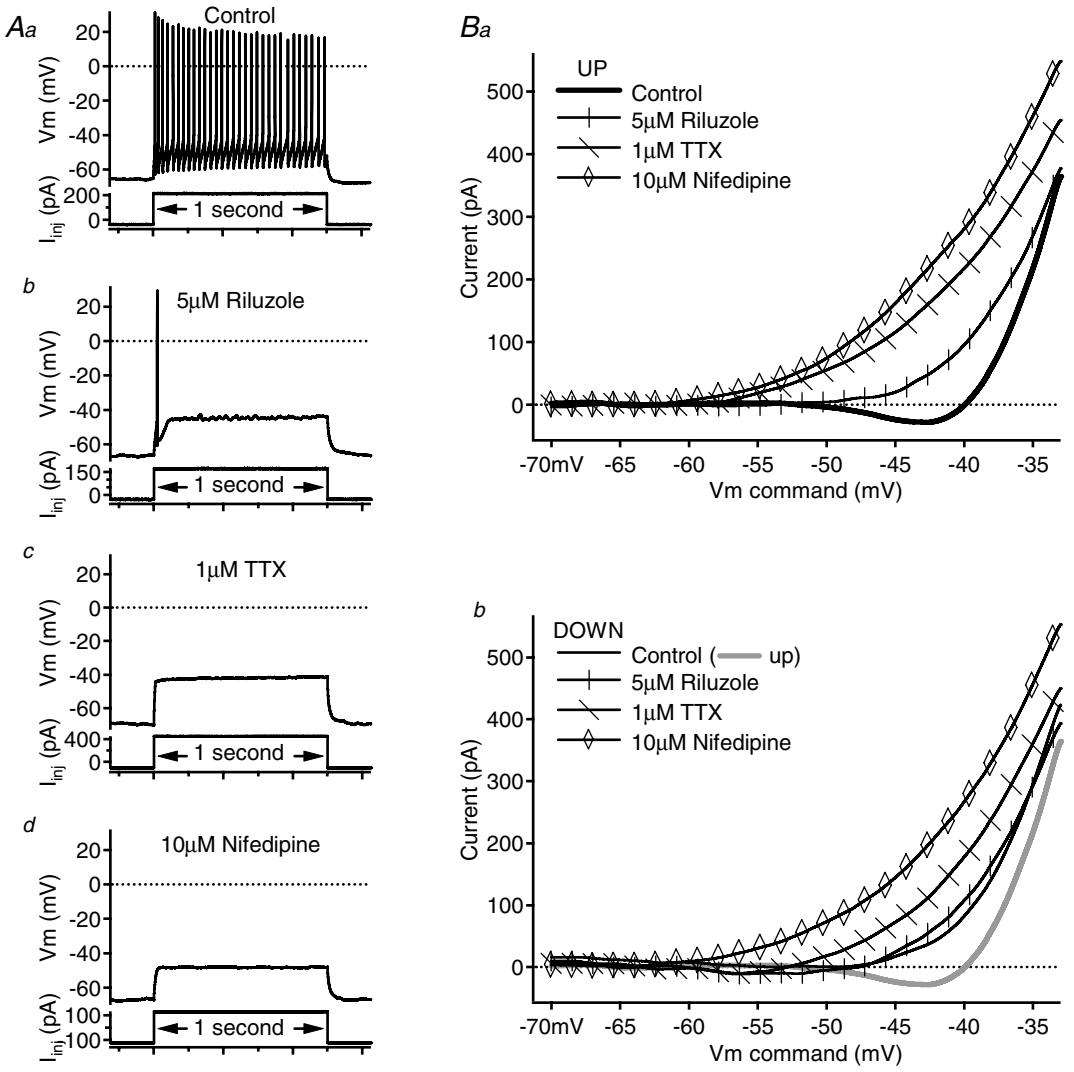

Figure 6. Contribution of Na_P and L-type calcium conductances to the PIC of a fully repetitive-firing cell
A, in the control condition (*Aa*), the cell fired repetitively to a 1 s, depolarizing current pulse. After 5 μM riluzole application (*Ab*), firing was reduced to a single spike. No spikes remained after 1 μM TTX application (*Ac*), and 10 μM nifedipine (*Ad*) produced little change in the response to the depolarizing step. In all of the panels, firing responses (membrane potential, V_m, in mV) are shown above the corresponding depolarizing, 1 s current pulses (I_{inj} in pA). *B*, in the leak-subtracted *I–V* relations, each subsequent drug application blocked more of the PIC on both the ascending (*Ba*) and descending (*Bb*) phases. Note that in the descending *I–V* (*Bb*) of this cell, the control and riluzole traces almost overlap. On the leak-subtracted *I–V* relations, the voltage command (in mV) is on the *x* axis and the current (in pA) is on the *y* axis; riluzole traces have vertical marks, TTX traces have diagonal marks and nifedipine traces have open diamond markers. Control traces are slightly thicker and unmarked. On the descending-phase *I–V* graph (*Bb*), the ascending control trace is also shown as a thicker, grey line.

Contribution of L-type Ca^{2+} currents

To evaluate the contribution of calcium currents to the different firing types, nifedipine, an L-type calcium channel antagonist, was bath applied after testing the effects of TTX. The concentration was high enough (10 μM) to strongly reduce the current from the $Ca_{V1.3}$ channels (Lipscombe *et al.* 2004), which are thought to mediate most of the Ca^{2+} component of the PIC (Li & Bennett, 2003). During nifedipine administration, bath application of TTX was continued, to maintain the elimination of sodium conductances. Overall, the nifedipine-sensitive current accounted for only 11.8% of the total ascending current blocked by TTX and nifedipine ($n = 11$), with no significant differences in this percentage among the different firing types. On the descending phase, the nifedipine-sensitive current accounted for 45.1% of the TTX + nifedipine current overall (fully repetitive: 30.6%, $n = 4$; repetitive/burst: 56.7%, $n = 3$; initial-burst: 50.7%, $n = 4$). Examples of the decrease in PIC with nifedipine application are also shown in Fig. 6 (repetitive-firing cell) and Fig. 7 (repetitive/burst cell). No significant differences

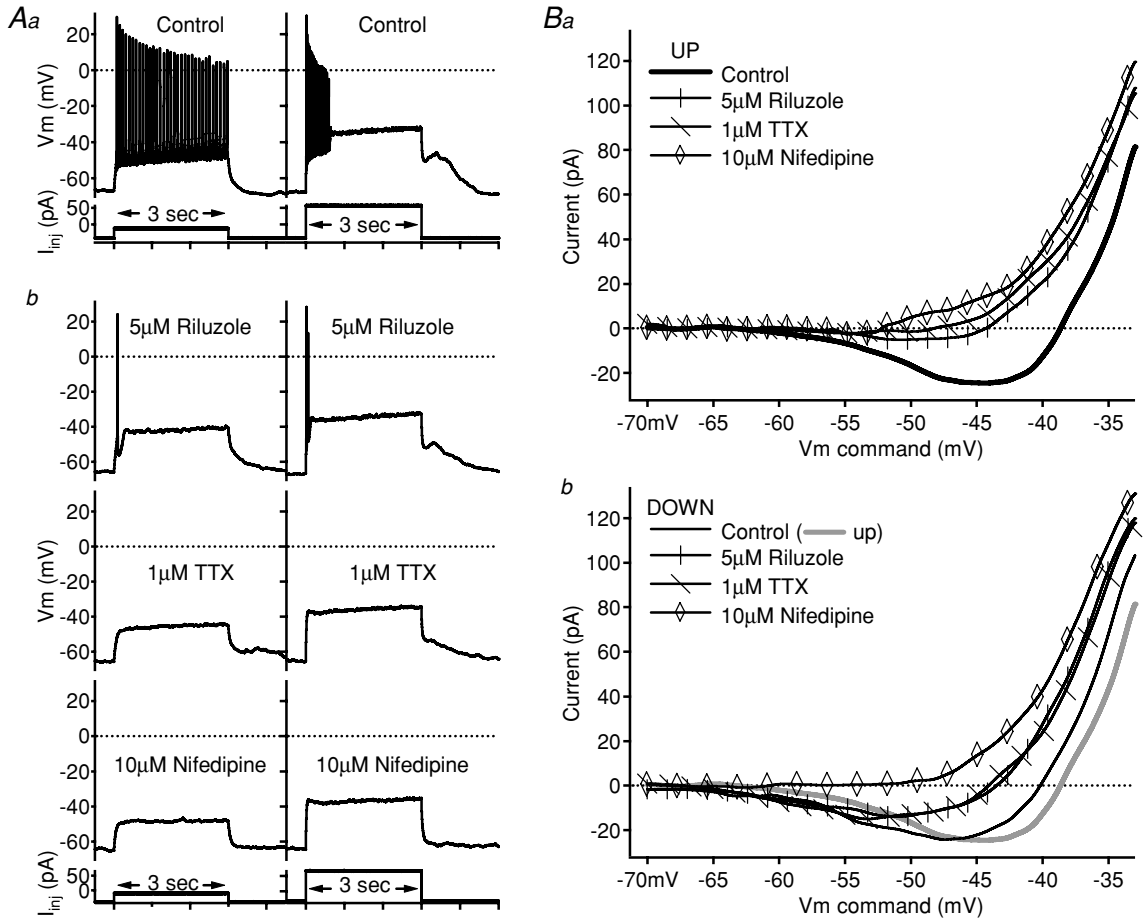

Figure 7. Contribution of Na_P and L-type calcium conductances to the PIC of a repetitive/burst cell
A, in the control condition (*Aa*), the cell fired repetitively to a 3 s depolarizing current pulse, but fired a high-frequency burst of spikes to a larger-amplitude 3 s pulse. After 5 μM riluzole application (*Ab*, top trace), firing was reduced to one spike for the smaller-amplitude pulse and two spikes for the larger-amplitude pulse. After 1 μM TTX application (*Ab*, middle trace), neither amplitude step produced spikes. The application of 10 μM nifedipine (*Ab*, bottom V_m trace) abolished this cell's post-step plateau. In *Aa* and *Ab*, firing responses (membrane potential, V_m, in mV) are shown above the corresponding depolarizing, 3 s current pulses (I_{inj} in pA). *B*, in the leak-subtracted *I–V* relations, each subsequent drug application blocked slightly more of the PIC on both the ascending (*Ba*) and descending (*Bb*) phases. Note that in the descending *I–V* (*Bb*) of this cell, the riluzole and TTX traces almost overlap, and the inward current remained. The application of 10 μM nifedipine finally eliminated the descending inward current (*Bb*, open diamonds). On the leak-subtracted *I–V* relations, the voltage command (in mV) is on the *x* axis and the current (in pA) is on the *y* axis; riluzole traces have vertical marks, TTX traces have diagonal marks and nifedipine traces have open diamond markers. Control traces are slightly thicker and unmarked. On the descending phase *I–V* graph (*Bb*), the ascending control trace is also shown as a thicker, grey line.

were observed in nifedipine-sensitive currents among the different firing types. Overall, these results show that Na_P dominates the PIC in ventral horn interneurones, but L-type Ca^{2+} also contributes.

Discussion

The primary results of this study are that PICs in ventral horn interneurones vary systematically with firing type, and that these PICs are predominantly generated by Na_P. Hence, it is likely that Na_P plays a major role in generating the differences in firing patterns among ventral horn interneurones. Administration of riluzole to progressively block Na_P converted repetitive-firing, repetitive/burst and initial-burst cells to the single-spiking pattern. This conversion of firing pattern suggests that the main difference between rhythmically firing interneurones and those exhibiting only single spikes is the lack of Na_P in the single-spiking cells. All interneurone firing types remained capable of producing spikes to brief steps following reduction of Na_P, showing that spike initiation to rapidly rising inputs remained intact. The loss of repetitive and burst firing probably occurs because Na_P plays a fundamental role in spike initiation to the relatively slowly rising depolarization provided by the decay of AHP during repetitive firing (see below). This role for Na_P is consistent with recent results in spinal motoneurones (Lee & Heckman, 2001; Kuo *et al.* 2006). Differences in Na_P, of course, do not account for all differences in firing patterns; a clear example in this study was that reducing Na_P to an

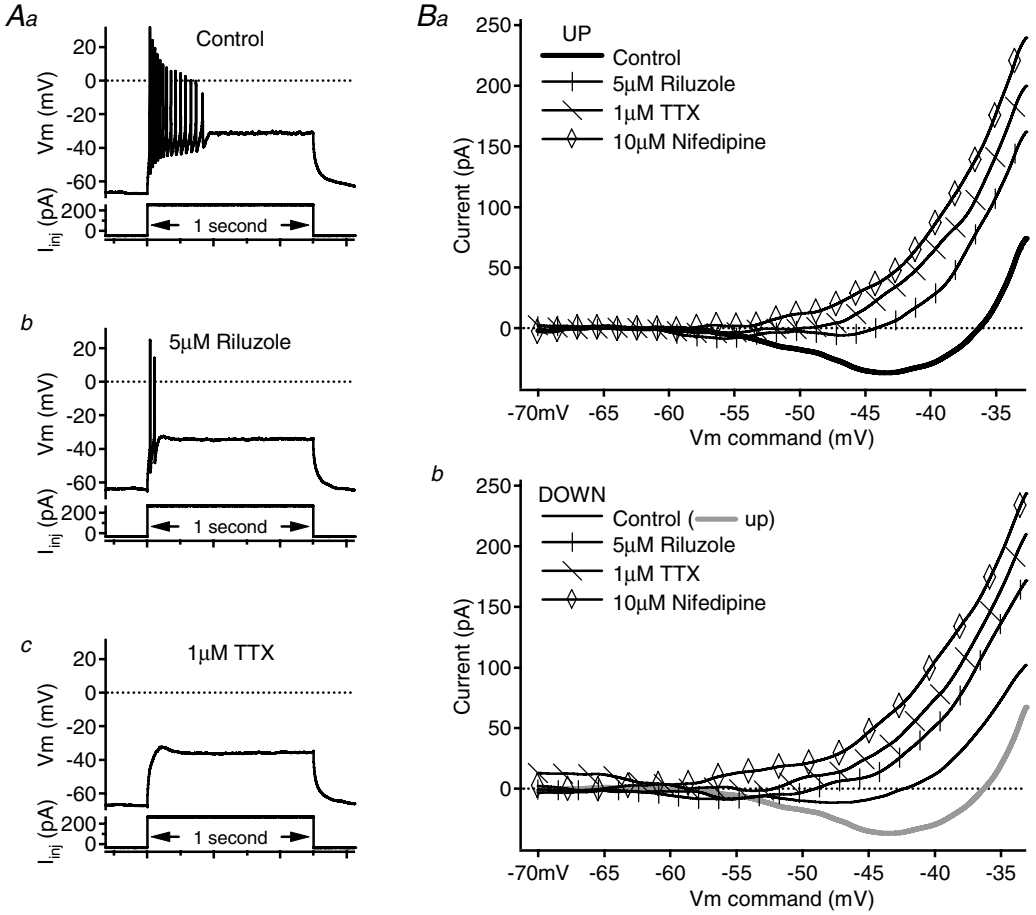

Figure 8. Contribution of Na_P and L-type calcium conductances to the PIC of an initial-burst cell
A, in the control condition (*Aa*), the cell fired a high-frequency burst of spikes to a 1 s depolarizing current pulse. A 5 μM riluzole application (*Ab*) reduced firing to two spikes, and 1 μM TTX application (*Ac*) eliminated the remaining spikes. In all of the panels, firing responses (membrane potential, V_m, in mV) are shown above the corresponding depolarizing, 1 s current pulses (I_{inj} in pA). *B*, in the leak-subtracted *I–V* relations, each subsequent drug application blocked more of the PIC on both the ascending (*Ba*) and descending (*Bb*) phases. On both panels, the voltage command (in mV) is on the *x* axis, and the current (in pA) is on the *y* axis; riluzole traces have vertical marks, TTX traces have diagonal marks and nifedipine traces have open diamond markers. Control traces are slightly thicker and unmarked. On the descending-phase *I–V* graph (*Bb*), the ascending control trace is also shown as a thicker, grey line.

intermediate level did not convert repetitive-firing cells to initial-burst patterns.

Limitations

As in our previous study (Theiss & Heckman, 2005), the synaptic blockers used in this preparation precluded functional identification using afferent inputs. This isolation from fast synaptic transmission had the advantage of assuring that we studied intrinsic cellular properties but eliminated the feasibility of associating firing patterns with functional identification as determined *in vivo* in the cat by Jankowska and colleagues (Jankowska, 1992, 2001; Jankowska & Hammar, 2002). Thus the issue of relating the type of sensory input these interneurones receive to their different firing patterns remains unresolved. It is also important to note that we, as others (Lopez-Garcia & King, 1994; Hochman *et al.* 1997; Garraway & Hochman, 2001; Prescott & De Koninck, 2002; Szucs *et al.* 2003; Theiss & Heckman, 2005), attempt to classify firing behaviours of cells, and that these firing behaviours may not indicate separable cell 'types.' For example, in the ventral horn, cells with predominant group I afferent input may display more than one firing behaviour. Additionally, under neuromodulatory conditions, certain cells may display different firing patterns than when not influenced by neuromodulators. For example, in the deep dorsal horn, Garraway & Hochman (2001) found that serotonin and noradrenaline as well as other neuromodulators tended to increase the number of spikes generated by single-spiking or initial-burst cells. These results could be in part explained by neuromodulatory actions on Na_P, i.e. facilitation of Na_P in initial-burst and single-spiking cells. Thus the importance of Na_P to the production of different firing patterns remains, especially if the firing behaviours of cells can be changed by neuromodulators. Further experiments are required to evaluate actions of neuromodulators on PICs and other intrinsic currents in spinal interneurones.

Thus far, studies of ventral horn interneurones in mammalian preparations have been done in neonatal and juvenile preparations. Smith & Perrier (2006) have found that all ventral interneurones in the adult turtle were capable of some type of repetitive firing. Cells with initial bursts or single spikes did not occur, and plateau potential behaviour was relatively common. These differences may reflect species differences but, given the similarity of the properties of turtle motoneurones (Alaburda *et al.* 2002) to rat and cat motoneurones (Heckman *et al.* 2005), the results of Smith & Perrier (2006) also suggest that Na_P may be more prevalent in the adult state and thus repetitive firing patterns more common. This does not seem to be the case in the dorsal horn, where initial-burst and single-spiking cells have been demonstrated *in vivo* in the adult mouse (Graham *et al.* 2004).

The portion of the sample exhibiting single-spiking patterns was smaller in this study than in our previous work (Theiss & Heckman, 2005). One possible factor contributing to this pattern is the use of whole-cell patch techniques (present study) compared to sharp electrodes (Theiss & Heckman, 2005). In addition to the differences in intracellular milieu with the two methods, sampling considerations are important. Our visualized patch-clamp approach in this work tended to bias the sample towards superficial cells. Single-spiking cells tend to have higher input conductances (Szucs *et al.* 2003). (A trend in this direction was also seen in the present study, but the sample size was too small – see Table 1.) Single-spiking interneurones may thus be relatively large and may survive best deep in the slice where their dendritic arborizations undergo less damage. These cells may thus have been under-sampled in the present study.

Importance of Na_P in spike initiation during repetitive firing

Na_P probably has a number of important effects on cell behaviour, including amplification and prolongation of synaptic input as well as subthreshold depolarization (Taddese & Bean, 2002; Li & Bennett, 2003; Li *et al.* 2004; Prescott & De Koninck, 2005). In addition, Na_P is likely to play a fundamental role in spike initiation during repetitive firing. Spike initiation requires an input with a rate of rise sufficiently fast for Na^+ channel activation to escape inactivation (Hille, 1992). This limitation does not apply to Na_P, and 'in fact' slow voltage ramps are the standard

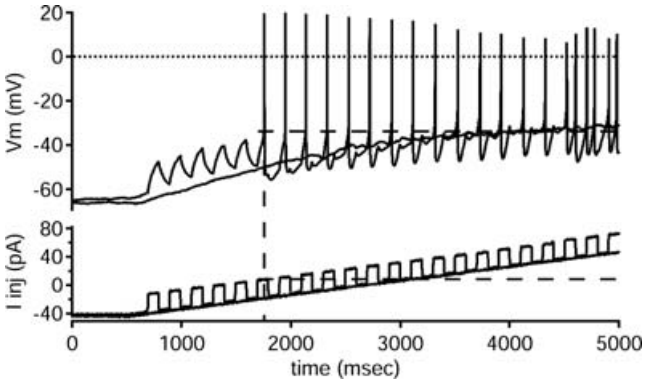

Figure 9. Riluzole's effect is not from transient sodium inactivation
Application of riluzole reduced repetitive, repetitive/burst and initial-burst firing patterns to 1–2 spikes. After 5 μM riluzole application, this cell did not fire (top trace, membrane potential, V_m, in mV) to a triangular ramp of injected current (bottom trace, I_{inj}, in pA). When short pulses were superimposed on the ramp (bottom trace), however, it responded with a spike to each pulse (top trace). If riluzole inactivated transient sodium currents, these repeated current pulses would not consistently produce spikes. This response was consistent in all 10 of the tested cells.

method of evoking Na_P independently of the full transient Na^+ current (Crill, 1996). In spinal motoneurones, the rate of depolarization provided by the AHP following each spike is slow enough that Na_P is required to provide sufficient acceleration to initiate the next spike in the train (Lee & Heckman, 2001; Kuo *et al.* 2006). Just as in motoneurones, reduction in Na_P with riluzole in our sample of ventral horn interneurones eliminated repetitive firing. A single spike remained at the onset of the input, where the rapid rate of rise was provided by the sharp onset of the current step. Also like motoneurones, increasing input current amplitude did not restore firing, but adding a series of pulses onto a ramp produced spikes even when repetitive firing to the ramp alone had failed. Thus, it is likely that Na_P plays an essential role in spike initiation in repetitive-firing interneurones as well as motoneurones. Given that riluzole also eliminated all but the first one or two spikes in initial-burst cells, it probably plays an essential role in generating most of the spikes in these cells' bursts.

Although we did not block I_K, our block of Na_P with riluzole was simple, repeatable, consistent and reliable with no odd behaviour. We conclude, then, that our subtractions provide a reasonable estimate of Na_P.

Previous interneurone studies have speculated about the currents underlying single-spiking and initial-burst firing patterns. The single-spiking pattern has been attributed to outward currents, such as a D-current (Wu & Barish, 1992), that, after one or two spikes, hyperpolarize the cell below spike voltage threshold (Ruscheweyh & Sandkuhler, 2002). Our results were consistent with those of Prescott and De Koninck (2005) who showed that in dorsal horn interneurones, single-spiking cells did not exhibit amplification of EPSPs and tended to have small

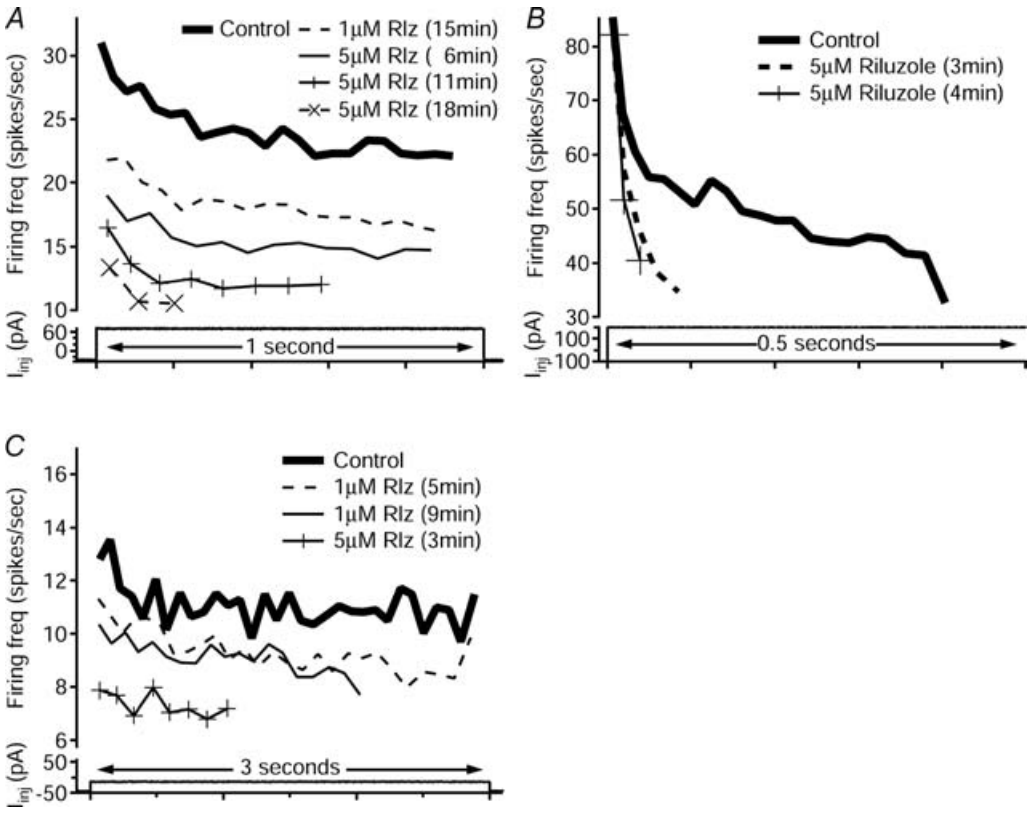

Figure 10. Changes in firing frequency–time (*f–t*) relations with riluzole application
Riluzole application had different effects on repetitive and burst frequency–time profiles. In all panels, firing frequency (Firing freq, top traces, in spikes s^{-1}) for control and riluzole traces is marked with the condition, concentration and duration of application. The frequency traces correspond to firing in response to a depolarizing current step (bottom traces) of indicated duration. *A*, when riluzole was applied to this repetitive-firing cell, firing frequency decreased with the same profile until spike failures were seen. Eventually, the input only produced one spike (not shown). This cell did not show a high-frequency initial-burst profile during the progression to a single spike. *B*, when riluzole was applied to this initial-burst cell, however, initial firing frequency remained the same, but the slope of the adaptation increased until the input only produced one spike (not shown). Note that only the first 0.5 s of the 1 s pulse is shown. *C*, when riluzole was applied to this repetitive/burst cell, changes in *f–t* relations mirrored those of the repetitive-firing cell in *A*. At the pulse amplitude that produced repetitive firing, the *f–t* relation maintained the same profile, but shifted downward during riluzole application.

amplitudes for Na_P when compared to repetitive-firing cells. Not ruling out the contribution of other currents, our results and those of Prescott & De Koninck (2005) suggest that single-spiking cells do not fire rhythmically because they lack Na_P.

Yet differences in Na_P cannot account for all differences in firing pattern among ventral interneurones. Decreasing Na_P in repetitive-firing interneurones did not reveal an intermediate state in which these cells exhibited initial-burst-type firing. Instead, repetitive firing was gradually reduced in frequency and then suddenly failed to a single-spiking pattern. We did not systematically vary the amplitude and holding potential during riluzole administration, to evaluate whether repetitive-firing cells went through a phase of repetitive/burst behaviour, yet initial-burst patterns were not seen during riluzole administration in any repetitive cell tested. Thus it is likely that lack of Na_P alone also does not account for the emergence of repetitive/burst behaviour. As suggested by Schneider (2003), initial-burst firing is probably mediated by several interacting conductances, and the same may be true for repetitive/burst cells. A T-type calcium current contribution is possible, especially given the high frequency of initial bursts, and this current has been found in rat dorsal horn neurones (Ryu & Randic, 1990; Russo & Hounsgaard, 1996). In our study, one further hint as to the mechanism of burst firing is that spike voltage threshold tended to be more depolarized in repetitive/burst and initial-burst cells than in repetitive-firing cells. This difference was small but significant. In contrast, PIC onset voltage was more depolarized in initial burst than repetitive/burst and repetitive cells. It is possible that the combination of depolarized spike threshold and PIC onset in initial-burst cells contributes to spiking that occurs in a depolarized region where activation of outward currents is stronger than in repetitive-firing cells. These outward currents may aid in burst termination. In repetitive/burst cells, more hyperpolarized PIC onset may partially compensate the depolarized spike threshold and allow repetitive firing in some input conditions.

Variations in repetitive-firing and bursting patterns have been seen in previous studies, including spike failures with large current steps or the development of repetitive firing from a burst with increasing-amplitude current steps (Jo *et al.* 1998; Ruscheweyh & Sandkuhler, 2002; Ruscheweyh *et al.* 2004). The repetitive/burst cells in this study that exhibited both kinds of firing behaviour appeared to be a true transition group between repetitive-firing and initial-burst cells, sharing PIC amplitude characteristics with the former, and PIC activation voltage properties with the latter. This group was also heterogeneous, with some cells exhibiting bursts with low-input step amplitudes and others with high amplitudes. It seems likely that different types of currents are involved in different repetitive/burst cells. Further study of mechanisms of burst behaviour in both repetitive/burst and initial-burst cells is required to resolve these issues.

Conclusion

Overall, our results support the hypothesis that strong PICs underlie repetitive firing to a prolonged or slowly rising input. Repetitive-firing cells had the largest PIC amplitudes that were mainly mediated by persistent sodium currents. Single-spiking cells had the smallest-amplitude PICs, and repetitive-firing neurones could be converted to single-spiking cells by simply blocking persistent sodium currents. Initial-burst and repetitive/burst cells had moderate-amplitude PICs, and the interplay of several ionic conductances probably accounts for these firing patterns. These results are significant in that they show that differences in one persistent current can contribute greatly to determining intrinsic firing patterns.

References

Alaburda A, Perrier JF & Hounsgaard J (2002). Mechanisms causing plateau potentials in spinal motoneurones. *Adv Exp Med Biol* **508**, 219–226.

Crill WE (1996). Persistent sodium current in mammalian central neurons. *Ann Rev Physiol* **58**, 349–362.

Derjean D, Bertrand S, Nagy F & Shefchyk SJ (2005). Plateau potentials and membrane oscillations in parasympathetic preganglionic neurones and intermediolateral neurones in the rat lumbosacral spinal cord. *J Physiol* **563**, 583–596.

Garraway SM & Hochman S (2001). Modulatory actions of serotonin, norepinephrine, dopamine, and acetylcholine in spinal cord deep dorsal horn neurons. *J Neurophysiol* **86**, 2183–2194.

Graham BA, Brichta AM & Callister RJ (2004). In vivo responses of mouse superficial dorsal horn neurones to both current injection and peripheral cutaneous stimulation. *J Physiol* **561**, 749–763.

Heckman CJ, Gorassini MA & Bennett DJ (2005). Persistent inward currents in motoneuron dendrites: implications for motor output. *Muscle Nerve* **31**, 135–156.

Heckman CJ, Lee RH & Brownstone RM (2003). Hyperexcitable dendrites in motoneurons and their neuromodulatory control during motor behavior. *Trends Neurosci* **26**, 688–695.

Hille B (1992). *Ionic Channels of Excitable Membranes*. Sinauer Associates, Sunderland, Mass.

Hochman S, Garraway SM & Pockett S (1997). Membrane properties of deep dorsal horn neurons from neonatal rat spinal cord in vitro. *Brain Res* **767**, 214–219.

Hultborn H, Brownstone RB, Toth TI & Gossard JP (2004). Key mechanisms for setting the input–output gain across the motoneuron pool. *Prog Brain Res* **143**, 77–95.

Jankowska E (1992). Interneuronal relay in spinal pathways from proprioceptors. *Prog Neurobiol* **38**, 335–378.

Jankowska E (2001). Spinal interneuronal systems: identification, multifunctional character and reconfigurations in mammals. *J Physiol* **533**, 31–40.

Jankowska E & Hammar I (2002). Spinal interneurones; how can studies in animals contribute to the understanding of spinal interneuronal systems in man? *Brain Res Brain Res Rev* **40**, 19–28.

Jo YH, Stoeckel ME & Schlichter R (1998). Electrophysiological properties of cultured neonatal rat dorsal horn neurons containing GABA and met-enkephalin-like immunoreactivity. *J Neurophysiol* **79**, 1583–1586.

Kuo JJ, Lee RH, Zhang L & Heckman CJ (2006). Essential role of the persistent sodium current in spike initiation during slowly rising inputs. *J Physiol* **574**, 819–834.

Lee RH & Heckman CJ (1998*a*). Bistability in spinal motoneurons in vivo: systematic variations in persistent inward currents. *J Neurophysiol* **80**, 583–593.

Lee RH & Heckman CJ (1998*b*). Bistability in spinal motoneurons in vivo: systematic variations in rhythmic firing patterns. *J Neurophysiol* **80**, 572–582.

Lee RH & Heckman CJ (1999). Paradoxical effect of QX-314 on persistent inward currents and bistable behavior in spinal motoneurons in vivo. *J Neurophysiol* **82**, 2518–2527.

Lee RH & Heckman CJ (2001). Essential role of a fast persistent inward current in action potential initiation and control of rhythmic firing. *J Neurophysiol* **85**, 472–475.

Li Y & Bennett DJ (2003). Persistent sodium and calcium currents cause plateau potentials in motoneurons of chronic spinal rats. *J Neurophysiol* **90**, 857–869.

Li Y, Gorassini MA & Bennett DJ (2004). Role of persistent sodium and calcium currents in motoneuron firing and spasticity in chronic spinal rats. *J Neurophysiol* **91**, 767–783.

Lipscombe D, Helton TD & Xu W (2004). L-type calcium channels: the low down. *J Neurophysiol* **92**, 2633–2641.

Lopez-Garcia JA & King AE (1994). Membrane properties of physiologically classified rat dorsal horn neurons in vitro: correlation with cutaneous sensory afferent input. *Eur J Neurosci* **6**, 998–1007.

Miles GB, Dai Y & Brownstone RM (2005). Mechanisms underlying the early phase of spike frequency adaptation in mouse spinal motoneurones. *J Physiol* **566**, 519–532.

Morisset V & Nagy F (1996). Modulation of regenerative membrane properties by stimulation of metabotropic glutamate receptors in rat deep dorsal horn neurons. *J Neurophysiol* **76**, 2794–2798.

Morisset V & Nagy F (1999). Ionic basis for plateau potentials in deep dorsal horn neurons of the rat spinal cord. *J Neurosci* **19**, 7309–7316.

Morisset V & Nagy F (2000). Plateau potential-dependent windup of the response to primary afferent stimuli in rat dorsal horn neurons. *Eur J Neurosci* **12**, 3087–3095.

Prescott SA & De Koninck Y (2002). Four cell types with distinctive membrane properties and morphologies in lamina I of the spinal dorsal horn of the adult rat. *J Physiol* **539**, 817–836.

Prescott SA & De Koninck Y (2005). Integration time in a subset of spinal lamina I neurons is lengthened by sodium and calcium currents acting synergistically to prolong subthreshold depolarization. *J Neurosci* **25**, 4743–4754.

Ptak K, Zummo GG, Alheid GF, Tkatch T, Surmeier DJ & McCrimmon DR (2005). Sodium currents in medullary neurons isolated from the pre-Botzinger complex region. *J Neurosci* **25**, 5159–5170.

Ruscheweyh R, Ikeda H, Heinke B & Sandkuhler J (2004). Distinctive membrane and discharge properties of rat spinal lamina I projection neurones in vitro. *J Physiol* **555**, 527–543.

Ruscheweyh R & Sandkuhler J (2002). Lamina-specific membrane and discharge properties of rat spinal dorsal horn neurones in vitro. *J Physiol* **541**, 231–244.

Russo RE & Hounsgaard J (1996). Plateau-generating neurones in the dorsal horn in an in vitro preparation of the turtle spinal cord. *J Physiol* **493**, 39–54.

Ryu PD & Randic M (1990). Low- and high-voltage-activated calcium currents in rat spinal dorsal horn neurons. *J Neurophysiol* **63**, 273–285.

Schneider SP (2003). Spike frequency adaptation and signaling properties of identified neurons in rodent deep spinal dorsal horn. *J Neurophysiol* **12**, 12.

Smith M & Perrier JF (2006). Intrinsic properties shape the firing pattern of ventral horn interneurons from the spinal cord of the adult turtle. *J Neurophysiol* **96**, 2670–2677.

Szucs P, Odeh F, Szokol K & Antal M (2003). Neurons with distinctive firing patterns, morphology and distribution in laminae V–VII of the neonatal rat lumbar spinal cord. *Eur J Neurosci* **17**, 537–544.

Taddese A & Bean BP (2002). Subthreshold sodium current from rapidly inactivating sodium channels drives spontaneous firing of tuberomammillary neurons. *Neuron* **33**, 587–600.

Theiss RD & Heckman CJ (2005). Systematic variation in effects of serotonin and norepinephrine on repetitive firing properties of ventral horn neurons. *Neuroscience* **134**, 803–815.

Thurbon D, Luscher HR, Hofstetter T & Redman SJ (1998). Passive electrical properties of ventral horn neurons in rat spinal cord slices [corrected and republished in *J Neurophysiol* 1998; 80: 2485–502] *J Neurophysiol* **79**, 2485–2502.

Urbani A & Belluzzi O (2000). Riluzole inhibits the persistent sodium current in mammalian CNS neurons. *Eur J Neurosci* **12**, 3567–3574.

Voisin DL & Nagy F (2001). Sustained L-type calcium currents in dissociated deep dorsal horn neurons of the rat: characteristics and modulation. *Neuroscience* **102**, 461–472.

Wu RL & Barish ME (1992). Two pharmacologically and kinetically distinct transient potassium currents in cultured embryonic mouse hippocampal neurons. *J Neurosci* **12**, 2235–2246.

Acknowledgements

This work was supported by NIH/NINDS NS40862 and NS034282 (C.J.H.). We are grateful to Dr Robert H. Lee for his technical assistance with programming data acquisition and conversion scripts and to Allison Hyngstrom for assistance with data collection.